Localising vibrating scatterer phenomena in synthetic aperture radar imagery

B. Corbett✉, D. Andre and M. Finnis

Artefact phenomena resulting from synthetic aperture radar (SAR) image formation can pose a challenge for image interpretation. One such artefact is produced when a vibrating target is imaged. Suppression of these artefacts has previously been described, however little has been developed in the area of modelling the location and shape of such artefacts. The authors present an experimentally validated model that provides accurate location and shape of vibrating target paired echoes in both SAR near-field and SAR far-field imagery.

Introduction: Synthetic aperture radar (SAR) is a proven radar data collection technique that is capable of producing high-resolution radar images from large stand-off distances [1]. However, SAR collections are susceptible to time-dependent effects including equipment and target variability, moving objects and other scene changes, all of which give rise to unwanted artefacts. This can often affect an image analyst's ability to understand the data they are reviewing. Of particular interest here are vibrating target paired echo artefacts, examples of which have been seen in both airborne and ground-based SAR images [2–5].

These artefacts arise as a result of imaging a target whose motion follows a periodic waveform during the SAR data collection [3, 6]. The motion of the target produces additional phase ramps across the phase (signal) history of the scatterer [3], resulting in the azimuthal smearing of the scatterer within a SAR image, producing the paired echo artefacts. The literature has described this effect as *micro-Doppler* [2, 7].

Little is understood of the precise location, form and shape of vibrating target artefacts in SAR imagery, particularly in SAR-near-field regime imagery. SAR far-field scenarios are more commonly considered because the flat wavefront assumption simplifies the analysis [8]. In the SAR near-field, spherical wave-fronts need to be considered, increasing the complexity [8]. A principle motivation to engage in the SAR near-field arises from the need to obtain higher signal powers for through-wall imaging, so that close proximity to the wall is desirable to overcome attenuation from wall materials [9].

The focus of this work is to formulate a model for computing the location and form of the paired echoes produced by vibrating targets within SAR imagery. The generalised model should operate for both the SAR near and far-field regimes. This paper provides an overview of the developed numerical model describing the precise form of vibration artefacts in SAR images. Validation results for the model from both simulated and experimental data are then presented.

Modelling vibrating target paired echoes: Cranfield University's GBSAR laboratory [10] operates a rail-based SAR system, the speed of the rail is low and constrained by the hardware. To measure vibrating target artefacts using the system, we present an approach for how the effects from any platform velocity and vibration frequency can be reproduced if an appropriate synchronisation between the scanner and the target is achieved, in effect resulting in a synthetic platform velocity and corresponding target vibration. In the following sections we formalise this approach by showing how dependencies on time can be replaced with dependencies on the relative positions of the platform and vibrating target alone.

Vibrating target paired echo phenomena are often described as the result of a micro-Doppler shift in the carrier frequency of the transmitted radar signal, caused by the displacement from the vibrating motion of a target [2, 7, 11]. How these artefacts appear in SAR imagery is therefore dependent upon both the positions of the target and the measurement platform throughout the SAR collection.

For a static antenna and target, the received radar pulse will have experienced a phase shift $\phi = 4\pi r/\lambda$, where λ is the wavelength of the transmitted signal and r is the range to target [8, 11]. If either the antenna or target is moving during the radar measurement, a Doppler frequency shift is experienced by the pulse caused by a change to the phase shift ϕ.

The Doppler frequency shift is given by $f_D = 2v/\lambda$, where v is the sum of the line of sight (LOS) velocity magnitudes between the measurement platform and the target, represented by v_1 and v_2 in Fig. 1 [7, 12].

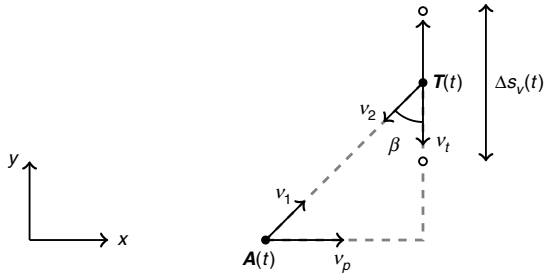

Fig. 1 *Model of velocity components used in calculating the Doppler frequency shift. The radar platform* $\boldsymbol{A}(t)$ *is moving with a velocity* v_p*. While a vibrating isotropic target* $\boldsymbol{T}(t)$ *has a reciprocating velocity* v_t *and results in a displacement of* $\Delta s_v(t)$*. The LOS velocity magnitudes are represented by* v_1 *and* v_2

We consider a target moving with a velocity v, in the frame of reference of the radar platform. The range to the target at time t is $r(t) = r(0) + \delta r(t)$, with $\delta r(t) = v\delta t$, representing the change in displacement of the target from its start position at $r(0)$. Therefore, the phase of a radar pulse is related to the Doppler frequency f_D as follows:

$$\phi(t) = \frac{4\pi}{\lambda}(r(0) + \delta r(t)) = \frac{4\pi r(0)}{\lambda} + 2\pi f_D \delta t \tag{1}$$

Equation (1) shows that the Doppler frequency shift term is linked to both a change in phase $\delta\phi$ and a change in displacement δr as follows [7, 13]:

$$f_D = \frac{2v}{\lambda} = \frac{2}{\lambda}\frac{\delta r}{\delta t} = \frac{1}{2\pi}\frac{\delta\phi}{\delta t} \tag{2}$$

This relationship shows that the Doppler frequency shift caused by the motion of a target can be determined solely through the analysis of the range between relative positions of the radar platform and target, thus removing the dependency on time. We use this knowledge to develop a model of the phase history data the GBSAR system would collect.

Now consider the scenario in Fig. 1 of a radar platform $\boldsymbol{A}$ moving with a velocity v_p along x (in cross-range), while an isotropic point scatterer $\boldsymbol{T}$ is vibrating perpendicular to the antenna trajectory along y (in range), with a displacement Δs_v. At time t the target position is $\boldsymbol{T}(t) = [\overline{T}_x(t), \overline{T}_y(t) + \Delta s_v(t), \overline{T}_z(t)]$, where $\overline{T}_x$, $\overline{T}_y$ and $\overline{T}_z$ are the mean x, y, z components of the target position.

We now assume a synthetic radar platform velocity v_s, such that for a given set of relative positions between the platform and the target, a synthetic vibration frequency for the target will arise. The corresponding synthetic time τ for the radar platform to traverse the measurement aperture of size, A_p, can be written as, $\tau = A_p/v_s$. Thus, the synthetic sampling time t is a function of the mth measurement position for N_p pulses

$$t(m) = \frac{m\tau}{N_p} = \frac{mA_p}{N_p v_s} \tag{3}$$

so that $\boldsymbol{A}$, $\boldsymbol{T}$ will become functions of the mth measurement position. The SAR phase history can now be written (ignoring scattering strength variation with range) as

$$\Phi(n, m) = \exp\left(i\frac{4\pi}{\lambda(n)}|\boldsymbol{A}(m) - \boldsymbol{T}(m)|\right) \tag{4}$$

where $\Phi(n, m)$ is the phase history for a single target located at a range $|\boldsymbol{A}(m) - \boldsymbol{T}(m)|$ at a synthetic time $t(m)$ and $\lambda(n)$ is the nth wavelength of each transmitted pulse.

The micro-Doppler effect captured in the phase history is now modelled and measured solely through the analysis of the variation in range between the vibrating target position and the SAR measurement position. Crucially, the platform does not have to be in actual motion for the micro-Doppler data to be collected, but the relative positions of radar platform and the vibrating target must be accurately controlled to create the micro-Doppler effect within the phase history.

Localisation model for vibrating scatterer artefacts: To locate vibrating target artefacts in SAR imagery, the effect of Doppler shift upon the spatial frequency domain is considered. The Doppler frequency from (1) gives rise to a periodic phase shift across the spatial frequency domain, which manifests itself as multiple orders of azimuthal phase ramps. Recalling that phase ramps in the Fourier domain give rise to shifts in the image domain, we now calculate the first-order phase ramp phase gradient.

In terms of the number of vibration cycles $f_v\tau$ and the extent of the data in spatial frequency F_w, the first-order phase ramp azimuthal phase gradient is $\nabla\phi = 2\pi f_v\tau/F_w$. In terms of the azimuthal resolution $\rho_a = c/2F_w$, this gives $\nabla\phi = 4\pi f_v\tau\rho_a/c$.

Now recalling that an azimuthal image domain shift D arises from a Fourier domain phase ramp with phase gradient $4\pi D/c$, it can be seen that the first-order artefact from the vibrating target will occur with an azimuth displacement [3, 8, 14]

$$D_v = \rho_a f_v \tau \tag{5}$$

D_v has previously been described as a straight line distance, measured parallel to the antenna trajectory, from the assumption of flat wave-fronts due to operation in the SAR far-field [8, 14]. However, due to the spherical nature of the radar wave-fronts, D_v is more correctly represented as an arc length at a constant range. With this modification, (5) can now be implemented for SAR near-field analysis. The scene is said to be in the SAR near-field when the range is less than $2L_{cr}^2/\lambda_c$, where L_{cr} is the SAR image cross-range extent and λ_c is the centre wavelength.

Fig. 2 visualises the artefact localisation. A vibrating isotropic point scatterer, whose mean location $\bar{\boldsymbol{T}}$ is located in the SAR near-field, with its first-order vibration artefacts is shown. The synthetic aperture is shown between its endpoints, $\boldsymbol{A}(0)$ and $\boldsymbol{A}(m)$. $R(m)$ is the antenna range to the mean position of the vibrating scatterer, such that $R(m) = |\boldsymbol{A}(m) - \bar{\boldsymbol{T}}|$. The two dotted lines indicate the extreme iso-ranges to the synthetic aperture end positions. The extents of the artefact in azimuth and range are denoted by S_a and S_r, respectively.

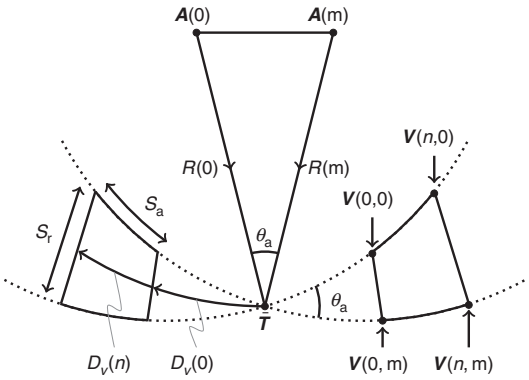

Fig. 2 *Vibrating target artefact model. Presenting the variables used in determining vibrating target artefact localisation and extent calculations*

In determining the extent of the first-order artefact, one may consider the wavenumber domain (k-Space), where the vibration artefact extent in the spatial domain is linked to the extent of the SAR image data in the wavenumber domain [3], so that S_r is determined by the synthetic aperture angle extent and S_a is determined by the transmitted bandwidth.

D_v can be made a function of the nth transmitted frequency sample, giving the arc length to any spatial position along the artefact azimuthal extent, hence from (5) and an approximation for azimuth resolution [14]

$$D_v(n) = \frac{\lambda(n)}{4\sin(\theta_a/2)} f_v\tau \tag{6}$$

Thus, the limits of the transmitted frequency range provide the smear azimuthal arc length is $S_a(n) = |D_v(0) - D_v(n)|$.

From this, the coordinate location for any position within the artefact extent can be calculated as follows:

$$\boldsymbol{V}(n, m) = [\boldsymbol{R}(\psi(n, m))(\bar{\boldsymbol{T}} - \boldsymbol{A}(m))] + \boldsymbol{A}(m) \tag{7}$$

where $\boldsymbol{R}$ is a 2D rotation matrix perpendicular to the slant plane of the collection, which uses an angle of rotation determined by $\psi(n, m) = D_v(n)/R(m)$. $\boldsymbol{R}$ is required to rotate the mean target coordinate location, $\bar{\boldsymbol{T}}$, around the endpoints of the synthetic aperture, $\boldsymbol{A}_1$ or $\boldsymbol{A}_2$, by the arc distance $D_v(n)$. In this way, (7) can be used to find the perimeter of the artefact extent.

Vibrating target artefacts are composed of multiple higher-order artefacts [5]. To find the location of the higher-order artefacts, it was found that $D_{vl} = lD_v$, where l is an integer, representing the order of the vibration artefact.

Model validation: As an initial validation of the model developed in (6) and (7), simulated vibrating point scatterers were examined, both in the SAR far-field and SAR near-field.

As an example, this displacement is modelled using a sinusoid waveform as a function of measurement position, $\Delta s_v(m) = A_v \sin(2\pi f_v t(m))$, where a 10 Hz vibration frequency f_v and a 5 mm amplitude A_v is applied. The scatterers for each simulation are located off-centre from the central broadside position to further test the model, and the vibration displacement is perpendicular to the direction of travel of the antennas.

Equation (4) was used to generate the simulated phase history data, using a bandwidth of 2 GHz with a centre frequency of 10 GHz, resulting in a range resolution of 75 mm. For the SAR far-field case, the measurement platform traversed a 100 m aperture with a synthetic velocity of 100 ms^{-1}, while for the SAR near-field case, the platform traversed a 2 m aperture with a synthetic velocity of 2 ms^{-1}.

Fig. 3 shows an example of simulated results formed in the slant plane projection, using the backprojection image formation algorithm [15], where Fig. 3*a* is the SAR far-field case and Fig. 3*b* is the SAR near-field case. The accuracy of the model is clearly shown through the superimposed plots of the echo localisation output overlaid onto the SAR images.

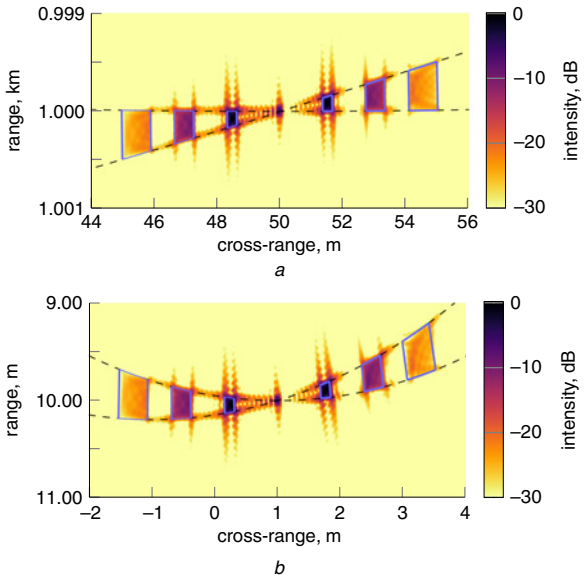

Fig. 3 *Simulated data showing vibrating target artefacts with predicted localisation superimposed. Each simulation features a single vibrating point scatterer, whose motion follows a sinusoidal waveform*

a SAR far-field simulation
b SAR near-field simulation

To provide vibrational artefacts in measurements, prior experimental methodology was implemented [4, 5]. To create the synthetic micro-Doppler effect in a controlled laboratory environment, a remote-controlled rover was developed capable of accurately moving small distances in synchrony with the radar scanner [4]. The experimental system behaviour is equivalent to the synthetic micro-Doppler model summarised in (4).

The following measurement scene was created, involving a single vibrating target located 11.3 m down-range of the synthetic aperture with 8 m scene width, so that the target was in the SAR near-field. The target was a 150 mm square trihedral mounted onto the rover, whose down-range displacement was given by $\Delta s_v(m) = A_v \sin(2\pi f_v t(m))$, using a 5 mm amplitude. Assuming a synthetic platform velocity of 2 ms^{-1} a vibration frequency 10 Hz could be measured.

The experimental data was gathered using a 3.5 m aperture, with the antennas mounted 2.79 m above the ground. The radar operated over a

2 GHz bandwidth with a centre frequency of 5.5 GHz, producing a 75 mm range resolution.

The data collected was formed into the two ground-plane projection SAR images seen in Fig. 4, using the backprojection image formation algorithm. Fig. 4*a* is the result from using the complete 3.5 m aperture data in the image formation, showing the target in a central broadside position; while Fig. 4*b* was formed using the left-most 2 m aperture data only, so that the target is off-centre from the central broadside position of the reduced collection aperture, making the target off-centre and comparable with the simulated results of Fig. 3.

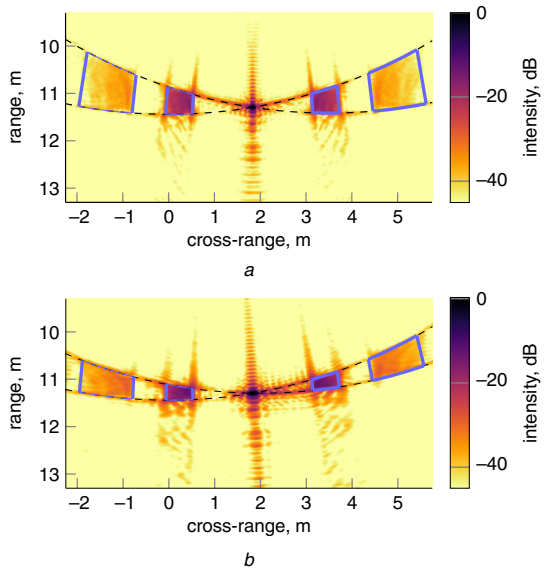

Fig. 4 *Experimental data showing vibrating target artefacts with predicted localisation superimposed. The target vibrational displacement follows a sinusoidal waveform*

a SAR image formed using the complete 3.5 m aperture
b SAR image formed using a 2 m sub-aperture, showing the target off-centre from the central broadside position

The output from the artefact localisation model is superimposed onto the SAR images in Fig. 4. The model has yielded an accurate localisation of the vibration artefacts in the experimental SAR images.

Conclusion: A detailed analysis of the localisation of the phenomena produced when imaging vibrating targets in SAR imagery has been presented. It was shown how synthetic micro-Doppler is equivalent to the micro-Doppler described in the literature. This equivalence allowed the measurement of vibrating target paired echoes corresponding to arbitrary synthetic radar platform speeds, using a low-speed laboratory scanner.

A technique was presented for accurately relating the localisation of the vibrating target paired echo phenomena in SAR imagery, with the vibrational properties of the target, which is applicable in both the SAR near and far-field regimes. The technique was validated with both simulated and experimental SAR images, with data collected at Cranfield University's GBSAR laboratory.

The investigation of vibrating target paired echo phenomena through this approach allows the inference of the vibration characteristics of the scatterer, due to the relationship between the artefact localisation and vibration frequency, providing useful target recognition intelligence from the SAR image.

Acknowledgments: The authors thank David Blacknell and Darren Muff for useful technical discussions on paired echo phenomena. This work was supported by DSTL.

Submitted: *18 December 2019* E-first: *5 February 2020*
doi: 10.1049/el.2019.4114
One or more of the Figures in this Letter are available in colour online.

B. Corbett and D. Andre (*Centre for Electronic Warfare, Information and Cyber, Cranfield University, Defence Academy of the United Kingdom, Shrivenham, Swindon SN6 8LA, United Kingdom*)

✉ E-mail: b.corbett@cranfield.ac.uk

M. Finnis (*Centre for Defence Engineering, Cranfield University, Defence Academy of the United Kingdom, Shrivenham, Swindon SN6 8LA, United Kingdom*)

References

1 Jakowatz, C.V Jr., Wahl, D.E., Eichel, P.H., *et al.*: 'Spotlight-mode synthetic aperture radar: a signal processing approach' (Kluwer Academic Publishers, Norwell, MA, USA, 1999, 1st edn.)
2 Chen, V.C., Li, F., Ho, S.S., *et al.*: 'Micro-doppler effect in radar: phenomenon, model, and simulation study', *IEEE Trans. Aerosp. Electron. Syst.*, 2006, **42**, (1), pp. 2–21, doi: 10.1109/TAES.2006.1603402
3 Andre, D., Blacknell, D., Muff, D., *et al.*: 'The physics of vibrating scatterers in SAR imagery'. Algorithms for Synthetic Aperture Radar Imagery XVIII', Orlando, FL, USA, May 2011, doi: 10.1117/12.883845
4 Corbett, B., Andre, D., and Finnis, M.: 'Through-wall detection and imaging of a vibrating target using synthetic aperture radar', *Electron. Lett.*, 2017, **53**, (15), pp. 991–995, doi: 10.1049/el.2017.1570
5 Corbett, B., Andre, D., Muff, D., *et al.*: 'Imaging SAR phenomenology of concealed vibrating targets'. 12th European Conf. on Synthetic Aperture Radar (EUSAR 2018), Archen, Germany, June 2018, pp. 1–5
6 Muff, D., Andre, D., Corbett, B., *et al.*: 'Comparison of vibration and multipath signatures from simulated and real SAR images'. Int. Conf. on Radar Systems (Radar 2017), Belfast, Northern Ireland, October 2017, pp. 1–6, doi: 10.1049/cp.2017.0396
7 Chen, V.C.: 'The micro-doppler effect in radar' (Artech House, Norwood, MA, USA, 2019, 2nd edn.)
8 Sullivan, R.J.: 'Microwave radar: imaging and advanced concepts' (Artech House, Norwood, MA, USA, 2000, 1st edn.)
9 De Wit, J.J.M., Van Rossum, W.L., Blacknell, D., *et al.*: 'Sensor technologies for seeing inside buildings an overview'. Remote Intelligence of Building Interiors (STO-MP-SET-247), Helsinki, Finland, February 2017, pp. 1–8, doi: 10.14339/STO-MP-SET-247
10 Andre, D., Morrison, K., Blacknell, D., *et al.*: 'Very high resolution coherent change detection'. 2015 IEEE Radar Conf. (RadarCon), Arlington, VA, USA, May 2015, pp. 634–639, doi: 10.1109/RADAR.2015.7131074
11 Chen, V.C., and Ling, H.: 'Time-frequency transforms for radar imaging and signal analysis' (Artech House, Norwood, MA, USA, 2002, 1st edn.)
12 Stimson, G.W., Griffiths, H.D., Baker, C.J., *et al.*: 'Stimson's introduction to airborne radar' (SciTech Publishing, Edison, NJ, USA, 2014, 3rd edn.)
13 Tait, P.: 'Introduction to radar target recognition' (The Institution of Engineering and Technology, Stevenage, UK, 2005, 1st edn.)
14 Carrara, W.G., Goodman, R.S., and Majewski, R.M.: 'Spotlight synthetic aperture radar, signal processing algorithms' (Artech House, Norwood, MA, USA, 1995, 1st edn.)
15 Munson, D.C., O'Brien, J.D., and Kenneth Jenkins, W.: 'A tomographic formulation of spotlight-mode synthetic aperture radar', *Proc. IEEE*, 1983, **71**, (8), pp. 917–925, doi: 10.1109/PROC.1983.12698